UNIVERSIDADE DE SÃO PAULO

INSTITUTO DE FÍSICA
CAIXA POSTAL 20516
01498 - SÃO PAULO - SP
BRASIL

publicações

IFUSP/P-460

STUDY OF PARTICLE EMISSION IN THE LIGHT-HEAVY ION FUSION REACTIONS: ^{14}N, $^{16,18}O + ^{12}C$

by

N. Carlin Filho, M.M. Coimbra, J.C. Acquadro, R. Liguori Neto, E.M. Szanto, E. Farrelly-Pessoa and A. Szanto de Toledo

Instituto de Física, Universidade de São Paulo

May/1984

STUDY OF PARTICLE EMISSION IN THE LIGHT-HEAVY ION FUSION REACTIONS: ^{14}N, $^{16,18}O + ^{12}C$

N.Carlin Filho[+], M.M.Coimbra[+], J.C.Acquadro, R.Liguori Neto, E.M.Szanto, E.Farrelly-Pessoa and A.Szanto de Toledo

Instituto de Física da Universidade de São Paulo
Departamento de Física Nuclear - Laboratório Pelletron
Caixa Postal 20516 - São Paulo,SP - CEP 01498 - BRASIL

ABSTRACT

From the energy spectra of light particles produced in light heavy ion induced reactions, level densities of the final nuclei as well as the critical angular momenta for fusion may be obtained.

The ^{14}N, $^{16,18}O + ^{12}C$ reactions were investigated in the energy range 30 MeV < E_{LAB} < 60 MeV. Detailed angular distributions of the light particles (p,d,t,α) emitted in the process were obtained.

Fits of the magnitude and shape of the spectra, by means of statistical model calculations were used to extract final nuclei level densities. The shape of the spectra and the ratio $\sigma(\alpha)/\sigma(p)$ are shown to be sensitive to the fusion critical angular momentum (J_{cr}), offering an alternative method for the total fusion cross-section determination.

[+]Supported by FAPESP

I. INTRODUCTION

The study of the emission of light particles in heavy ion reactions is currently of great interest and provides a powerful tool for the understanding of various features of the reaction mechanisms[1-4]. In particular, information on the fusion cross-section limitation, the time evolution of heavy ion collisions and the mechanism of energy and angular momentum dissipation may be obtained.

Evaporation and non equilibrium products have been identified in a very wide energy region spanning the Coulomb barrier up to relativistic energies[1-5]. Systematics on particle energy distributions, nuclear temperatures (level densities) and effective fusion barriers, as well as detailed angular distributions leading to information on the nuclear angular momenta are becoming available.

The interpretation of these experiments depends upon the assumed reaction mechanism and in the compound nucleus case, the degree with which the light particles are emitted from statistically equilibrated composite systems[6].

For light heavy ion collisions $A \leq 40$, at energies just above the Coulomb barrier, the formation of an equilibrated compound nucleus is the most probable process and statistical theories are suited for the description of the formation and subsequent sequential decay of the compound nucleus.

The probability for the formation of specific residues (final nuclei) depends on the competition between the different possible emitted particles, i.e. the number of open exit channels. This probability is very closely related to the angular momentum distribution of the compound nucleus which is determined mainly by the critical angular momentum for fusion (J_{cr}) and the final nuclei level densities.

At present little information is available on s-d nuclei level densities and most of it is obtained via neutron scattering experiments and low-energy light particle induced reactions[7,8].

The critical angular momenta for fusion of s-d nuclei, obtained mainly by the residues detections technique[9], reflect in this mass region, the uncertainties due to the difficulties in associating the residues with a specific reaction mechanism.

In this paper, we propose the use of heavy ion compound reactions to extract, on the basis of statistical theories, level densities of s-d nuclei as well as the fusion cross section, from the observation of the light charged particles emitted in the process.

The absolute double differential cross-sections $d^2\sigma/d\Omega dE^*$ reflect directly the J-critical value. This is manifested through the dependence of the magnitude on the excitation energy E^* of the residual nucleus, the level density

and also in the anisotropy of the angular distribution[10].

If the composite system reaches the statistical equilibrium before the emission of the light particles, this emission may be described in terms of statistical windows[11] in the angular momentum space. Within this framework, it is clear that the lightest particles are emitted preferencially from the low angular momentum components of the compound nucleus. On tne other hand, the heaviest particles, sensitive to the highest ℓ-partial waves, will be consequently sensitive to the limiting angular momentum J_{cr} for the compound nucleus formation.

The ratios of the emission cross sections σ of heavy to light particles e.g. $\sigma(\alpha)/\sigma(n)$ or $\sigma(\alpha)/\sigma(p)$ are therefore determined by the J_{cr} value. On the other hand, the dependence of these ratios on the entrance channel and decay width (i.e. the denominator of the Hauser-Feshbach expression[10]) will be strongly attenuated when compared to their effect on the magnitude of the cross section (σ).

In the present paper the (^{14}N, $^{16,18}O$) + ^{12}C reactions were investigated detecting light particles (p,d,t,^{3}He,α, (n)[12]) in order to determine level densities in the final nuclei and obtain cross section for complete fusion. Fits of the double differential cross sections to statistical model prediction are used to justify the reaction mechanism.

II. THE EXPERIMENT

Beams of $^{14}N(E_{LAB} = 46$ MeV), $^{16}O(E_{LAB} = 48.8$ MeV and 54.2 MeV) and $^{18}O(E_{LAB} = 41.3$ MeV) were provided by the University of São Paulo Pelletron tandem accelerator. Angular distributions of light particles were measured, using self supporting natural carbon targets of $\sim 30\ \mu g cm^{-2}$ thick, in the angular internal of $5^{o} \lesssim \theta_{LAB} \lesssim 90^{o}$ in $\Delta\theta = 5^{o}$ steps. Two solid state detector telescopes, were used to identify the light particles; the ΔE detectors were about 20 μm and 40 μm thick and the E detectors 1000 μm and 2000 μm thick. Nickel absorber foils of 13.8 mg/cm^2 were used in front of the telescopes to stop the elastically scattered particles as well as fusion residues thus, reducing the dead time at forward angles. A typical energy resolution of $\sim$ 100 keV was achieved, and was due mainly to the target thickness and kinematical broadening. Normalization of the absolute cross sections was performed by using a monitor detector at $\theta_{LAB} = 15^{o}$ and measuring an angular distribution of the elastic scattering at a sub Coulomb energy ($E(^{16}O) = 18$ MeV). Beam current integration at the scattering chamber Faraday cup was also done.

The ΔE and E energy signals were recorded in the event mode and replayed in the $(\Delta E) \times (E_T = E + \Delta E)$ matrix. It is important to note that the energy resolution is highly improved when the projection is performed onto the $E + \Delta E$ axis (see

fig. 1.a,b). The energy calibration was found linear using the discrete states populated selectively in the $^{12}C(^{16}O,\alpha)^{24}Mg$ reaction (see fig. 2) as well as the $H(^{16}O,H)^{16}O$ and $H(^{16}O,\alpha_o)^{13}N$ reactions. Corrections due to energy loss of the light particles in the Ni absorber foils were taken into account.

Double differential cross sections $d^2\sigma/d\Omega dE^*$ were obtained for all emitted particles, as a function of angle for excitation energy intervals $dE^* = 1.0$ MeV, from our spectra linearized in excitation energy. The angular distributions for the continuum are shown in fig. 3 and were calculated for energies $E^* > 9$ MeV. These values give an estimate of the region of overlap of the final nuclei levels defined by the relation $D(E^*) = \frac{1}{\rho(E^*)} \sim \Gamma(E^*)$ where $D(E^*)$ is the average energy level spacing and $\Gamma(E^*) = 14.6\exp(-4.69\sqrt{A/E^*})$ represents the average width of levels at an excitation energy E^*[13].

Experimental angle integrated cross sections $d\sigma/dE^* = \int \frac{d^2\sigma}{d\Omega dE^*} d\Omega$ were calculated by fitting the angular distributions with a sum of Legendre Polynomials $\frac{d^2\sigma}{d\Omega dE^*}(\theta) = \sum_\ell A_\ell P_\ell(\cos\theta)$ and equating $\frac{d\sigma}{dE^*}$ to $4\pi A_o$ (see fig. 3).

Experimental uncertainties of the order of 10% to 15% are attributed mainly to the determination and uniformity of of the target thickness and, in the case of the unfavoured decay channels, to the counting statistics.

The total cross section for a given exit channel (b) within an excitation energy interval $\Delta E^* = E^*_{MAX} - E^*_o$ can be

estimated

$$\sigma_b(\Delta E^*) = \int_{E_o^*}^{E_o^* + \Delta E^*} \frac{d\sigma}{dE^*}$$

In order to compare the experimental results with statistical model calculation in which a single decay is described, the energy limits E_o^* and $E_o^* + \Delta E^*$ must be correctly estimated to be able to extract reliable level density parameters as well as critical angular momenta.

III. COMPARISON OF THE SPECTRA AND ANGULAR DISTRIBUTIONS WITH STATISTICAL MODEL PREDICTIONS

In the energy region investigated in the present work, the compound nucleus emission is expected to be the dominant process, and therefore the comparison of the data with statistical model predictions should be adequate. This expectation is confirmed by the anisotropy of the angular distributions.

In order to extract accurate values for level density parameters for the final nuclei, it is important to guarantee that only the first chance decay is considered and no relevant contribution of sequential decay is present in the portion of the spectrum to be compared to the theoretical calculations.

Initially, the experimental spectra were qualitatively

compared to the predictions of the Monte-Carlo Hauser-Feshbach code LILITA[14] in which standard parameters were used (see fig. 4). To facilitate this comparison, calculated spectra of one particle decay mode, evaluated by the code STATIS[15], were also obtained in order to determine the energy region in which sequential decay is negligible. These results are supported by binding energy considerations and particle emission thresholds.

After the establishment of the E_o^* and $E_o^* + \Delta E^*$ energies within which only one particle decay is present, the experimental cross sections are compared to the Hauser-Feshbach calculations (performed with the code STATIS) in which the level density parameters and critical angular momenta are adjustable parameters.

The formalism of the statistical model can be found elsewere, e.g.,ref.16-18. To simplify the discussion, however, some of the most important expressions used are listed below.

The angle integrated cross section for the excitation of an individual state with spin I_B at excitation energy E_B^* in the reaction A(a,b)B is

$$\sigma(E_B^*, I_b) = \sum_{J=0}^{J_{cr}} \sigma_{CN}(J) G(E_B^*, I_B)/g(J) = \sum_{J=0}^{J_{cr}} \sigma_J(E_B^*, I_b) \qquad (1)$$

where the compound nucleus formation cross section

$$\sigma_{CN}(J) = \pi \lambda_1^2 \frac{2J+1}{(2I_A+1)(2I_a+1)} \sum_{S_1} \sum_{L_1} T_{L_1}(E_a) \qquad (2)$$

The partial and total decay widths of the compound nucleus are given respectively by

$$G(E_B^*, I_B, J) = \sum_{S_2} \sum_{L_2} T_{L_2}(E_B^*) \tag{3a}$$

$$g(J) = \sum_{b'} \sum_{L_2'} \sum_{S_2'} \sum_{I_B^*} \int_0^{E_{B'Max}} T_{L_2'B'}(E_{B'}^*, I_{B'}) \rho(E_{B'}^*, I_{B'}) dE_{B'}^* \tag{3b}$$

(all the symbols are defined in ref. 10).

The evaluation of the total decay width g(J), as well as the emitted particle spectrum, requires the knowledge of the energies, spins and parities of all final states and channels (b') into which the compound nucleus may decay. Since usually only a few low-lying levels are known, a level density expression is employed for higher excitation energies. The Fermi-gas expression[7,8,19] is expected to describe correctly the level density at higher excitation energies and has been used in the present work:

$$\rho(E^*, I) = (2I+1)\exp\left[-I(I+1/2)^2/2\sigma^2\right]\rho(E^*) \tag{4a}$$

where

$$\rho(E^*) = \frac{\exp(2(aU)^{1/2})}{12a^{1/4}(U+t)^{5/4}(2\sigma^2)^{3/2}} \tag{4b}$$

and the nuclear temperature t is related to the intrinsic excitation

energy $U = E^* - \Delta$ corrected for the pairing energy Δ and level density parameter $\underline{a}$ by:

$$U = at^2 - t$$

The spin-cutoff parameter σ depends on both excitation energy and moment of inertia, $\Theta = 2/5\ mAR^2 = \frac{2}{5}\ r_y^2 A^{5/3}$, through the relation:

$$\sigma^2 = \Theta t/\hbar^2 \qquad (4c)$$

A cutoff is imposed on the level density by the Yrast line in the residual nuclei estimated from

$$E^{Yrast}(I) = \frac{\hbar^2}{2\Theta}[I(I+1)-K^2] \qquad (5)$$

The expressions for the differential cross sections are given by the relation[15-18]

$$\frac{d\sigma}{d\Omega}(\theta, E_B^*, I_B) = \frac{\lambda_1^2}{4(2I_A+1)(2I_a+1)} \sum_{\substack{L_1 L_2 L \\ S_1 S_2 \\ J}} (-1)^{S_2-S_1} \times$$

$$\times P_L(\cos\theta) \frac{T_{L_1} T_{L_2}}{g(J)} \times \bar{Z}(L_1 J L_1 J | S_1 L) \bar{Z}(L_2 J L_2 J | S_2 J) \qquad (6)$$

The double differential cross section for an energy

bin dE^* at an excitation energy E^* is then evaluated by the relation

$$\frac{d^2\sigma}{d\Omega dE^*}(\theta) = \sum_{I_B=0}^{I_{Yrast}} \sum_{J=0}^{J_{cr}} \frac{d\sigma_J}{d\Omega}(\theta, E^*, I_B)\rho(E^*, I_B) \qquad (7)$$

and the angle integrated cross section is then given by

$$\frac{d\sigma}{dE^*} = \sum_{I_B=0}^{I_{Yrast}} \sum_{J=0}^{J_{cr}} \sigma_J(E_B^*, I_B)\rho(E_B^*, I_B) = \sum_{J=0}^{J_{cr}} \sigma_J(E_B^*) \qquad (8)$$

III.1. Determination of the Level Densities

When the Fermi-gas model is used, the level density parameter $\underline{a}$ can be written as[8]

$$a = [0.00917(S(Z) + S(N)) + b]A$$

where S(Z) and S(N) are proton and neutron shell corrections and b is a constant which depends on the nuclear symmetry. If shell corrections are unavailable, a very rough, uniform expression a = A/constant may be used. Facchini et al.[7] proposed a value of a = A/8 for the uniform level density parameter.

In order to extract a uniform value for s-d nuclei,

from the present work, the shape of the α,p,d, and t spectra from the ^{14}N, ^{16} ^{18}O + ^{12}C reactions were fitted simultaneously using a common level density. It is clear that the shape of the spectra as well as the partial decay widths for all decay channels are essentially governed by the final nucleus level density and critical angular momentum. The total cross section

$$\sigma_b(\Delta E^*) = \int_{E_o^*}^{E_o^* + \Delta E} \frac{d\sigma}{dE^*}\, dE^* \qquad (9)$$

corresponding to the exit channel b, has also been fitted to the data.

No satisfactory fits to the data were obtained using a uniform level density parameter i.e. a = A/constant. Figure 5 shows the results for the α,p,d exit channels of the ^{12}C + ^{16}O system. Consequently the level density parameters were treated as independent free parameters for the different channels with the condition that the same value for a has been used for a given final nucleus regardless of how it has been populated.

Initially the reduced radius r_y, associated with the moment of inertia (eq.4c), has been adjusted by fitting the anisotropy of the angular distribution (see fig. 3). The parameters used in the present calculations are listed in tables 1-3. The fits of the angle integrated cross sections $\sigma_b(\Delta E^*)$ for all the channels

(fig. 6) provided a first estimate of adequate level density parameters. However a finite set of parameters that give equivalent fit quality can be obtained. The individual and simultaneous fit of the shape and magnitude of all exit channels observed in all the reactions investigated removes this ambiguity (see fig. 7).

It is important to note that the α and p channels determine essentially the magnitude of the Hauser-Feshbach denominator g(J). The third important channel, the neutron emission, has been investigated only in the $^{12}C + ^{16}O$ case[12], and the results have been used only as guides for the cross-section normalization.

The d and t channel have very reduced effects on the overall agreement of the fits determining only the shape of the explicit channel.

The final results are listed in table 4 and are compared to values found in the literature. The uncertainties quoted in table 4 reflect the statistical uncertainties, the parameter ambiguities, the non explicit consideration of the neutron channel and finally, small possible discrepancies when different sets of optical model parameters are used.

III.2. Determination of the Critical Angular Momentum and Fusion Cross-Section

Complete fusion cross-sections of light heavy ion collisions and associated critical angular momenta are determined essentially by the measurement of the cross section for the formation of evaporation residues. In this section we show how the study of the spectra of particles emitted in the light heavy ion reactions also allows the extraction of this information.

The analysis of the expressions 1 to 3 together with the fact that, in heavy ion reactions, the grazing angular momentum of the emitted particle (ℓ_g) is small compared to the one in the entrance channel (L), indicates that the population of high spin states (E*,I) in the final nucleus is favored by the high angular momentum components (σ_J) of the compound nucleus[10,11]. The population probability of the final states is consequently determined essentially by "statistical windows"[11] in the angular momentum space (see fig. 8).

The truncation of the partial cross section sum (eq. 1) by the critical angular momentum J_{cr} substantially affects the high spin state cross sections whereas the low spin states remain unaffected[10] (see fig. 8). This fact has two major consequences. First, the anisotropy of the angular distributions of the continuum will be attenuated as the excitation energy increases

due to an increase of the "average spin of the continuum". Second, the excitation energy dependence of the anisotropy is directly related to the shape of the spectra and therefore related to the critical angular momentum.

The fact that the "statistical windows" are centered essentially at a J-value equivalent to the emitted particle plus the channel spin ($\langle J \rangle = \ell_g^b + S^b$) clearly shows that the windows for light emitted particle channels (i.e. n or p) will be centered at a much lower value than the window associated to the heavier exit channel (i.e. α or Li), for equivalent final excitation energies (see fig. 8).

An important consequence of this fact is that the cross sections for different emitted particles will be affected differently by the J_{cr} cutoff and therefore, the ratio of the cross sections of a heavy particle channel with respect to a light one is very sensitive to the critical angular momentum for compound nucleus formation. These arguments underlie the method proposed in the present work for determining J_{cr}.

As has been shown previously, the description of the spectra as well as the integrated cross sections are also strongly dependent on the level densities not only for the channel under consideration but for all the possible decay channels included in the Hauser-Feshbach denominator g(J) as shown by the relationship

$$\sigma(\Delta E^*) = \int_{E_o}^{E_o^*+\Delta E^*} \sum_J \sigma_{CN}(J) \frac{\sigma(E_b^*, I_b, J)}{g(J)} \rho(E_b^*, I_b) dE^* \qquad (10)$$

In order to by pass the strong dependence of the results in the level density it can be seen from figure 9 that the relative value of the cross sections for a heavy particle channel compared to a lighter one i.e. $R = \sigma_{\alpha}(\Delta E^*)/\sigma_{p}(\Delta E^*)$ is also highly sensitive to the critical angular momentum for fusion. Thus a fit of the ratio R has the advantage that most of the dependence on the level density is removed since the total decay width is the same for both channels.

χ^2-fits to the experimental absolute cross sections were performed using the sharp cutoff approximation in eq. 2 and 3 along with a difuseness described by writing the compound nucleus formation as:

$$\sigma_{CN} = \pi\lambda^2 \sum_{\ell=0}^{\infty} (2\ell+1) T_{\ell} P_{\ell} \qquad (11a)$$

where

$$P_{\ell} = \frac{1}{1 + \exp \frac{\ell - \ell_{cr}}{\delta_{\ell}}} \qquad (11b)$$

represents the probability with which the ℓ-partial wave contributes to the fusion after the barrier penetration. The χ^2-fits summarized in figures 10 and 11 were calculated using the expression:

$$\chi^2 = \frac{1}{N-1} \sum_{i} \left(\frac{\sigma(\Delta E_i^*)^{exp} - \sigma(\Delta E_i^*, J_{cr})^{HF}}{\epsilon_{\Delta E_i^*}} \right) \qquad (12a)$$

where $\sigma(\Delta E_i^*)^{exp}$, $\sigma(\Delta E_i^*)^{HF}$ and $\varepsilon_{\Delta E_i^*}$ represent respectively the experimental and Hauser-Feshbach cross sections for a bin of excitation energy ΔE_i^* in the spectrum, and $\varepsilon_{\Delta E_i^*}$ the experimental uncertainty.

If the shape only of the spectrum is fitted the relation

$$\chi^2 = \frac{1}{N-1}\left\{\sum_i \left|\frac{\sigma(\Delta E_i^*)^{exp} - \delta(J_{cr})\sigma(\Delta E_i^*)^{HF}}{\varepsilon_{\Delta E_i^*}}\right|\right\}_{Min} \qquad (12b)$$

has to be minimized by varying the normalization factor $\delta(J_{cr})$. The discrepancy and sensitivity of the fits shown in figure 10, is very closely related to the exact knowledge of the level densities.

On the other hand, the fit of the ratio of cross sections $R = \sigma_\alpha/\sigma_p$ shows rapid convergence to a J_{cr} value which is in agreement with the one obtained by means of evaporation residue method (see fig. 11). The complete fusion cross-section can be deduced using the relations 11a,b where the experimental value of ℓ_{cr} in considered in equation 11b. The comparison of the results from the present work with the fusion cross-sections obtained by means of evaporation residues technique[9] is shown in figure 12.

IV. CONCLUSION

The study of charged particle emissions in light heavy ion reactions has been shown to be of capital importance in the identification of the reaction mechanism. A careful analysis of the continuum spectra as well as the double differential cross sections $d^2\sigma/d\Omega dE^*$ reveals clearly the time evolution of the system and allows the extraction of important inclusive quantities such as the averaged level densities and critical angular momenta for complete fusion.

The statistical analysis of the spectra produced by the decay of an equilibrated compound nucleus has been used to extract, in the case of the ^{14}N, $^{16,18}O$ + ^{12}C reactions, level densities of s-d nuclei populated in at very high excitation energies. The use of a microscopic description for the level densities calculated realistically in the context of the statistical model may be extended to investigate the dependence of the level density parameters on the excitation energy well as the angular momentum distribution determined by the spin cutoff parameter.

The investigation of the bombarding energy dependence of the emission of heavy particles compared to the emission probability of lighter ones ($\sigma(\alpha,Li)/\sigma(n,p)$) can supply an alternative method for the determination of the critical angular momentum of the compound nucleus and consequently the fusion

cross section. This alternative can be very useful in the investigation of light-heavy ion fusion reactions in which the evaporation of few particles leaves projectile like residues which are easily confused with the products of quasi-elastic processes.

FIGURE CAPTIONS

Figure 1. Two-dimensional E-ΔE spectra for the systems ^{14}N, $^{16,18}O + {}^{12}C$. From the upper plots we can note the elimination of the slope in the discrete transitions, and consequently an improvement in the resolution, when we have in the x-axis $E_T = (E + \Delta E)$ (upper right) instead of E (upper left). The contours of constant Z, from top to bottom, correspond to the α-particles, ^{4}He, ^{3}He, t, d and p, respectively.

Figure 2. Spectrum of the $^{12}C(^{16}O,\alpha)^{24}Mg$ reaction, measured at $E_{LAB} = 54.2$ MeV, $\theta_{LAB} = 8.5^{o}$. The high spin selectivity of this reaction was explored for calibration. The dotted line corresponds to a polinomial fit for the continuum.

Figure 3. Experimental angular distributions for some excitation energy intervals in the continuum referring to exit channels for the system $^{12}C + {}^{16}O$ ($E_{LAB} = 54.2$ MeV). The solid lines correspond to the theoretical calculations performed with the code STATIS[15], in the region where the sequential decay contribution is negligible. The dashed curves corresponding to the region that includes the sequential decay, were normalized.

Figure 4. Comparison of some experimental spectra (dots) with the predictions of the Monte-Carlo code LILITA (histogram).

Figure 5. Total cross sections, $\sigma_{\Delta E^*}$, for the main exit channels referring to the system $^{12}C + ^{16}O$ (E_{LAB} = 54.2 MeV), as a function of a/A. The dashed horizontal lines correspond to the experimental values of $\sigma_{\Delta E^*}$, associated with their uncertainties. We can note by the observation of the thin solid lines (calculations) that there no values of a/A adjusting simultaneously $\sigma_{\Delta E^*}$ for all channels.

Figure 6. Fits of magnitude for $\sigma_{\Delta E^*}$ referring to the three systems $^{12}C + ^{14}N, ^{16,18}O$. The dots are the experimental values and the vertical lines, the theoretical calculations. The level density parameters used in the calculations, are listed in tables 1-3.

Figure 7. Shape and magnitude simultaneous fits for the angle integrated spectra, to all investigated reactions. The dots are the experimental values, the solid lines correspond to the calculations for region ΔE^* (the dashed lines correspond to the regions where the sequential decay contribution is important. We clearly note, in this region, the deviation from the experimental spectra).

Figure 8. Partial cross section $\sigma_J(E^*,I)$ for the excitation of final states with different spins, for the reactions $^{12}C(^{16}O,\alpha)^{24}Mg$ and $^{12}C(^{16}O,p)^{27}Al$. J corresponds to the angular momentum of the compound nucleus. The dashed vertical line corresponds to the experimental critical angular momentum for this reaction. The dashed curve corresponds to the "statistical windows" of the continuum (ΔE^* = 1 MeV) at the indicate excitation energy.

Figure 9. Cross sections $\sigma_{\Delta E^*}$ versus J_{cr}, for the systems investigated in the present work. The solid lines are the theoretical calculations. The triangles and the dots correspond to the experimental values $\sigma_{\Delta E^*}$ for the α-particles and protons, respectively.

Figure 10. χ^2-fits of the absolute cross sections and the shape of the spectra. The solid lines correspond to the absolute cross section fits and the dotted-dashed lines, to the shape fits of the spectrum using equation 12b.

Figure 11. Fits for the ratio $R = \sigma_\alpha(\Delta E^*)/\sigma_p(\Delta E^*)$, using the relation

$$\delta^2 = \left[\frac{R_{exp}(\Delta E^*) - R^{HF}_{\Delta E^*}(J_{cr})}{\varepsilon_R}\right]^2 .$$

Figure 12. Fusion cross sections (σ_F) values calculated with the values of J_{cr} obtained from the χ^2-fits. The dots are related to the fits of the ratio. The triangles and squeres correspond to the J_{cr} value obtained from the absolute cross sections for α-particles and protons fits, respectively. The open circles correspond to the experimental values of σ_F from Kovar et al.[9].

	$^{16}O + ^{12}C$	$n + ^{27}Si$	$p + ^{27}Al$	$d + ^{26}Al$	$t + ^{25}Al$	$\alpha + ^{24}Mg$
V_o	$7.5 + 0.4E_{CM}$ [a]	$56.3 - 0.32E_{CM} -$ $-24(N-Z)/A$ [b]	$49.9 - 0.22E_{CM} +$ $+26.4(N-Z)/A + 0.4Z/A^{1/3}$ [b]	$91.13 + 2.2Z/A^{1/3}$	$151.9 - 0.17E_{CM} +$ $+50(N-Z)A$ [b]	125.3 [b]
r_o	1.35	1.17	1.16	1.05	1.20	1.55
a_o	0.45	0.75	0.75	0.86	0.72	0.54
W_v	$0.4 + 0.125E_{CM}$ [a]	$0.22E_{CM} - 1.56$ [b]	$1.2 + 0.09E_{CM}$ [b]	-	$41.7 - 0.33E_{CM} +$ $+44(N-Z)/A$ [b]	30.7 [b]
r_v	1.35	1.26	1.37	-	1.40	1.59
a_v	0.45	0.58	$0.74 - 0.008E_{CM} +$ $+ (N-Z)/A$	-	0.88	0.39
W_S	-	$13.0 - 0.25E_{CM} -$ $- 12(N-Z)/A$ [b]	$4.2 + 0.05E_{CM} +$ $+15.5(N-Z)/A$ [b]	$218/A^{2/3}$	-	-
r_S	-	1.26	1.37	1.43	-	-
a_S	-	0.58	$0.74 - 0.008E_{CM} +$ $+ (N-Z)/A$	$0.5 + 0.013/A^{2/3}$	-	-
R_c	1.35	-	1.25	1.30	1.30	1.30
Δ	5.0 [c]	2.09 [c]	1.80 [c]	0.0 [c]	2.67 [c]	5.13 [c]
r_Y	1.40	1.40	1.40	1.40	1.40	1.40
Q_o(MeV)	0.0	-0.42	5.17	-5.67	-10.77	6.77

TABLE 1. Optical model and statistical model parameters for the system $^{16}O + ^{12}C$

a) Ref. 21 b) Ref. 22 c) Ref. 8

	$^{14}N + ^{12}C$	$n + ^{25}Al$	$p + ^{25}Mg$	$d + ^{24}Mg$	$t + ^{23}Mg$	$\alpha + ^{22}Na$
V_o	$7.5 + 0.4E_{CM}$ [a]	$56.3 - 0.32E_{CM} - 24(N-Z)/A$ [b]	$49.9 - 0.22E_{CM} + 26.4(N-Z)/A + 0.4Z/A^{1/3}$ [b]	$91.13 + 2.2Z/A^{1/3}$	$151.9 - 0.17E_{CM} + 50(N-Z)/A$ [b]	125.3 [b]
r_o	1.35	1.17	1.16	1.05	1.20	1.55
a_o	0.45	0.75	0.75	0.86	0.72	0.54
W_v	$0.4 + 0.125E_{CM}$ [a]	$0.22E_{CM} - 1.56$ [b]	$1.2 + 0.09E_{CM}$ [b]	-	$41.7 - 0.33E_{CM} + 44(N-Z)/A$ [b]	30.7 [b]
r_v	1.35	1.26	1.37	-	1.40	1.59
a_v	0.45	0.58	$0.74 - 0.008E_{CM} + (N-Z)/A$	-	0.88	0.39
W_S	-	$13.0 - 0.25E_{CM} - 12(N-Z)/A$ [b]	$4.2 + 0.05E_{CM} + 15.5(N-Z)/A$ [b]	$218/A^{2/3}$	-	-
r_S	-	1.26	1.37	1.43	-	-
a_S	-	0.58	$0.74 - 0.008E_{CM} + (N-Z)/A$	$0.5 + 0.013/A^{2/3}$	-	-
R_c	1.35	-	1.25	1.30	1.30	1.30
Δ	5.0 [c]	2.67 [c]	2.46 [c]	5.13 [c]	2.46 [c]	0.0 [c]
r_Y	1.40	1.40	1.40	1.40	1.40	1.40
Q_o(MeV)	0.0	3.71	8.77	3.66	-6.62	5.62

TABLE 2. Optical model and statistical model parameters for the system $^{14}N + ^{12}C$

a) Ref. 21 b) Ref. 22 c) Ref. 8

	$^{16}O + ^{12}C$	$n + ^{29}Si$	$p + ^{29}Al$	$d + ^{28}Al$	$t + ^{27}Al$	$\alpha + ^{26}Mg$
V_o	17.0	$47.01-0.26E_{CM}$	$56.09-0.55E_{CM}$	$81.0-0.22E_{CM}$	147.1	99.9
r_o	1.35	1.34	1.25	1.15	1.40	1.5
a_o	0.57	0.66	0.65	0.81	0.61	0.60
W_v	7.19	-	-	-	54.1	11.3
r_v	1.35	-	-	-	1.40	1.50
a_v	0.57	-	-	-	0.61	0.60
W_S	-	$9.52-0.053E_{CM}$	13.5	$14.4+0.24E_{CM}$	-	-
r_S	-	1.28	1.25	1.34	-	-
a_S	-	0.48	0.47	0.68	-	-
R_c	1.35	-	1.25	1.15	1.4	1.5
Δ	5.0[a]	2.09 [a]	1.67 [a]	0.0 [a]	1.80 [a]	4.26[a]
r_γ	1.40	1.40	1.40	1.40	1.40	1.40
Q_o(MeV)	0.0	13.039	10.141	2.93	1.46	13.008

TABLE 3. Optical model[23] and statistical model parameters for the system $^{16}O + ^{12}C$

a) Ref. 8

Nucleus	$a(MeV^{-1})$*	A/a(MeV)	$a(MeV^{-1})$+
^{22}Na	4.11 ± 0.08	5.35	3.13 [a]
^{23}Mg	4.37 ± 0.07	5.26	-
^{24}Mg	4.03 ± 0.04	5.96	3.32[a], 3.48[c]
^{25}Mg	4.13 ± 0.06	6.05	3.85[a], 3.70[c]
^{26}Mg	4.37 ± 0.07	5.95	4.08 [a]
^{25}Al	4.63 ± 0.09	5.40	3.54 [b]
^{26}Al	3.51 ± 0.03	7.41	3.65 [a]
^{27}Al	3.92 ± 0.08	6.89	3.45[a], 4.90[c]
^{28}Al	4.00. ± 0.04	7.00	-
^{29}Al	4.26 ± 0.06	6.81	4.08 [a]

TABLE 4. Level density parameters

* Present work

\+ Results found in the literature

a) Ref. 8 b) Ref. 7 c) Ref. 20

REFERENCES

1. R.G. Stokstad, M.N. Nanboodiri, E.T. Chulik, J.B. Natowitz and D.L. Hanson - Phys.Rev. C16 (1977) 16.

2. M.N. Nanboodiri, P. Gonthier, M. Mo, J.B. Natowitz, R. Eggers, L. Adler, P. Kasiraj, C. Cerruti, A. Chevarier, N. Chevarier and A. Demeyers - Nucl.Phys. A367 (1981) 313.

   P.L. Gonthier, M. Mo, M.N. Nanboodiri, J.B. Natowitz, L. Adler, S. Simon, K. Magel, S. Kniffen and A. Khodai - Nucl.Phys. A411 (1983) 289.

3. R. Billerey, C. Cerruti, A. Chevarier, N. Chevarier, B. Cheynes, A. Demeyer and M.N. Nanboodiri - Phys.Rev.Lett. 47 (1981) 639.

4. D. Logan, M. Rajagopalon, M.S. Zisman, J.M. Alexander, M. Kaplan and L. Kowalsky - Phys.Rev. C22 (1980) 104.

   D. Logan, H. Delagrange, M.F. Rivet, M. Rajagopalon, J.M. Alexander, M. Kaplan, M.S. Zisman and F. Duek - Phys.Rev. C22 (1980) 1080.

5. C.K. Gelbke, C. Olmer, M. Buenerd, D.L. Hendrie, J. Mahoney, M.C. Mermaz and D.K. Scott - Phys.Rep. 42 (1978) 313.

   A. Menchaca-Rocha, M.E. Brandan, M. Buenerd, J. Chauvin,

D. Lebrun, P. Martin, P. de Santignon, J.C. Gondrand, I. Dorion and A. Hounis - Phys.Lett. 131B (1983) 31.

6. P. Stwertka, T.M. Cormier, M. Herman, N. Nicolas, A. Szanto de Toledo, M.M. Coimbra and N. Carlin Filho - Phys.Rev.Lett. 49 (1982) 640.

7. N. Facchini and E. Saetta-Menichella - En.Nucl. 15 (1968) 54.

8. A. Gilbert and A.G.W. Cameron - Con.Journ.Phys. 43 (1965) 1446.

9. D.G. Kovar, D.F. Geesaman, T.H. Braid, Y. Eisen, W. Henning, T.R. Ophel, M. Paul, K.E. Rehm, S.J. Sanders, P. Sperr, J.P. Schiffer, S.L. Tabor, S. Vigdor, B. Zeidman and F.W. Prosser Jr. - Phys.Rev. C20 (1979) 1305.

Y.D. Chan, D.E. Di Gregorio, J.L.C. Ford Jr., J. Gomez del Campo, M.E. Ortiz and D. Shapira - Phys.Rev. C25 (1982) 1410.

D.E. Di Gregorio, J. Gomez del Campo, Y.D. Chan, J.L.C. Ford Jr., D. Shapira and M.E. Ortiz - Phys.Rev. C26 (1982) 1490.

10. A. Szanto de Toledo, M. Schrader, E.M. Szanto, G. Rosner and H.V. Klapdor - Nucl.Phys. A315 (1979) 500.

E.M. Szanto, A. Szanto de Toledo, H.V. Klapdor, G. Rosner and M. Schrader - Nucl.Phys. A404 (1983) 142.

11. M.S. Hussein and A. Szanto de Toledo - Phys.Lett. 107B (1981) 173.

12. M.C.H.M. Ruiz, R.A. Douglas, H.R. Schelin, J.L. Cardoso Jr., E.W. Cybulska and E. Farrelly-Pessoa - IFUSP Annual Report 1981 & Private comunication.

13. D. Shapira, R.G. Stokstad and D.A. Bromley - Phys.Rev. C10 (1974) 1063.

14. J. Gomez del Campo and R.G. Stokstad - Monte Carlo Code LILITA ORNL-TM 7295 - unpublished.

15. R.G. Stokstad - Wright Nuclear Structure Laboratory Yale University - Internal Report - nº 52 (1972).

16. T. Ericson - Ann. of Phys. 23 (1963) 390.

T. Ericson and T. Mayer-Kuckuk - Ann.Rev.Nucl.Sci. 16 (1966) 183.

17. T.D. Thomas - Ann.Rev.Nucl.Sci. 18 (1968) 343.

18. E. Vogt - Adv. in Nucl.Phys. 1 (1968).

19. J.M.B. Lang and K.J. Le Couteur - Proc.Soc.Lond. A67 (1954) 586.

20. E. Erba, U. Facchini and E. Saetta-Menichella - Il Nuovo

Cim. 22 (1961) 1237.

21. R. Singh, K.A. Eberhard and R.G. Stokstad - Phys.Rev. C22 (1980) 1971.

22. C.M. Perey and F.G. Perey - Nucl. Data Tables 13 (1974) 293 and 10 (1972) 539.

23. D.E. Gustafson, J. Gomez del Campo, R.L. Robinson, P.H. Stelson, P.D. Miller and J.K. Bair - Nucl.Phys. A262 (1976) 96.

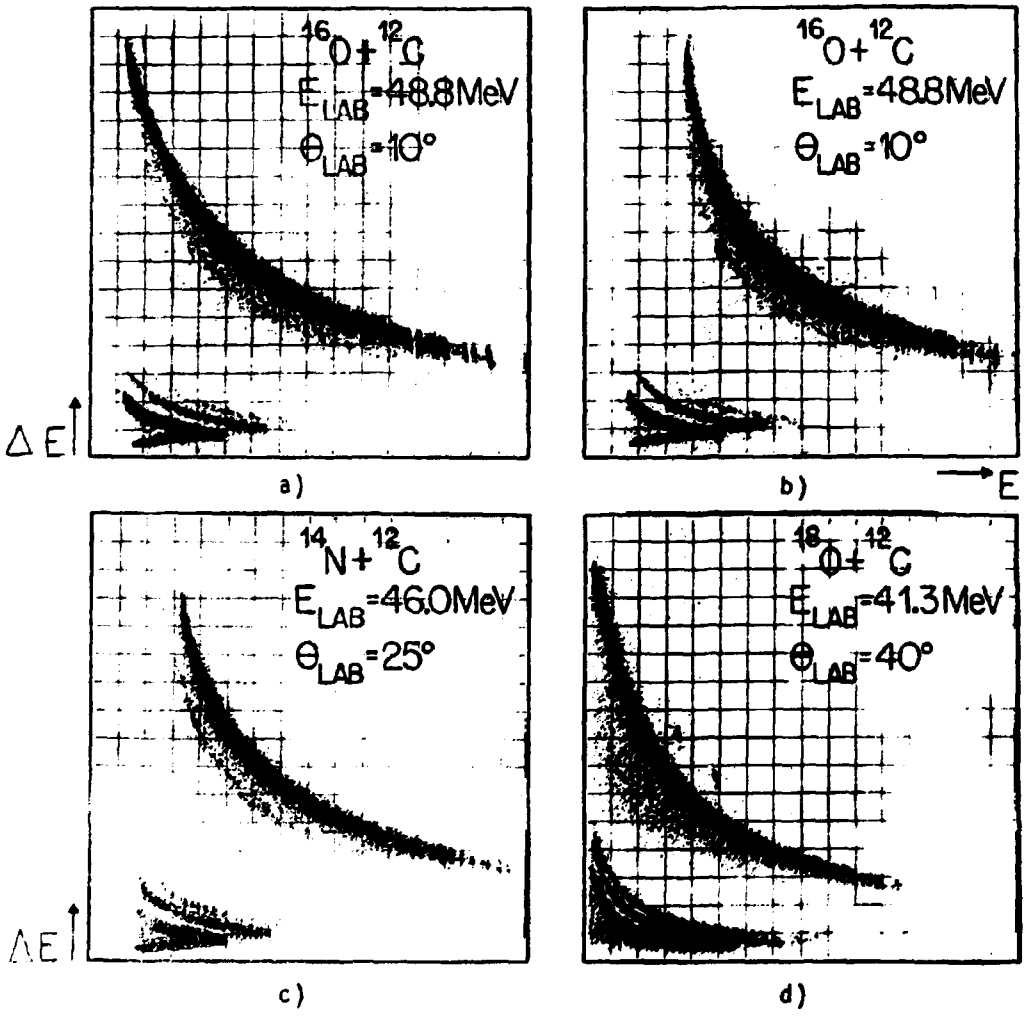
$^{16}O + ^{12}C$
E_{LAB}=48.8MeV
θ_{LAB}=10°
ΔE
a)
$^{16}O + ^{12}C$
E_{LAB}=48.8MeV
θ_{LAB}=10°
E
b)
$^{14}N + ^{12}C$
E_{LAB}=46.0MeV
θ_{LAB}=25°
ΔE
c)
$^{18}O + ^{12}C$
E_{LAB}=41.3MeV
θ_{LAB}=40°
d)

Fig. 1

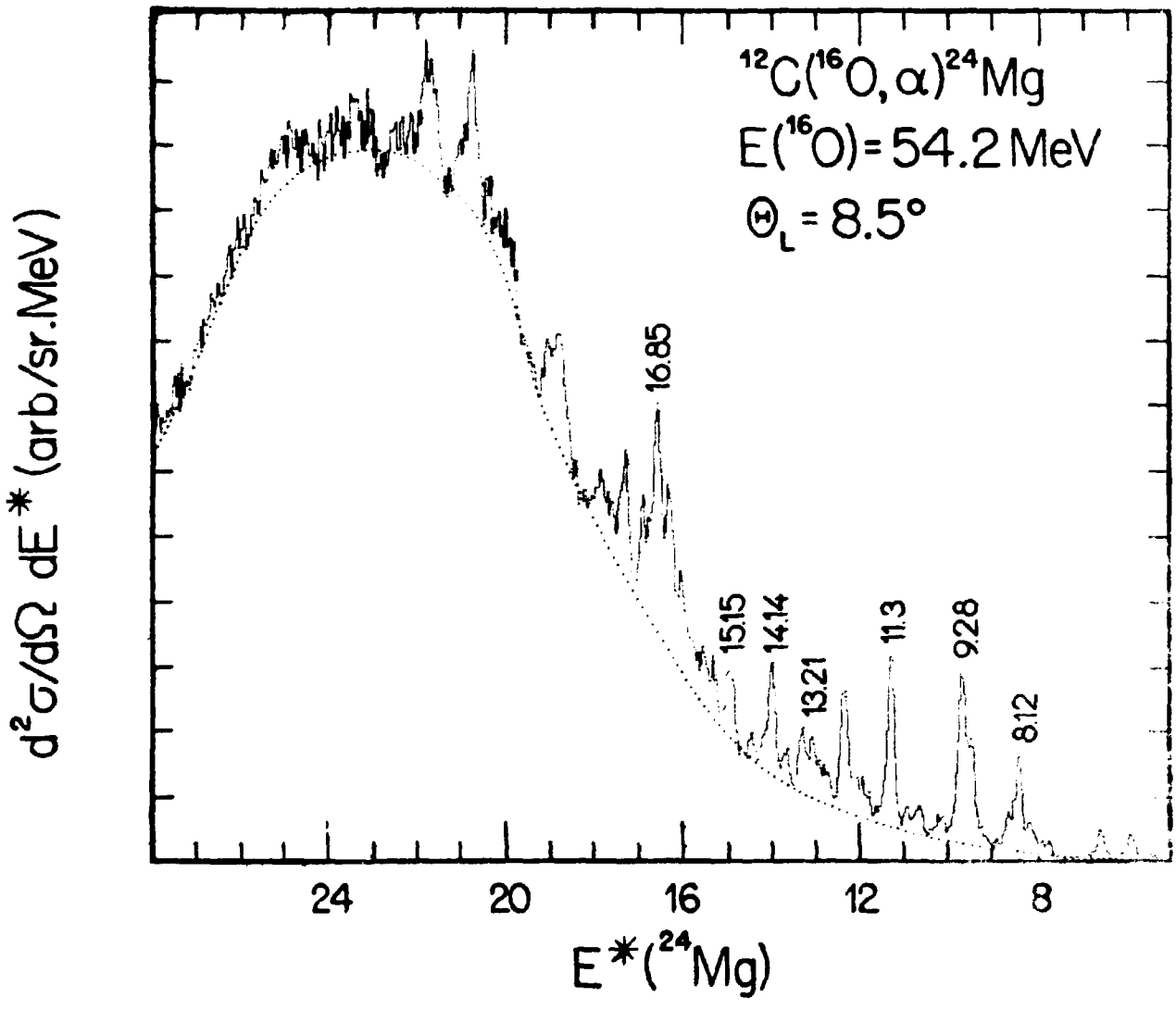
$^{12}C(^{16}O,\alpha)^{24}Mg$
$E(^{16}O) = 54.2\,MeV$
$\Theta_L = 8.5°$
16.85
15.15
14.14
13.21
11.3
9.28
8.12
24
20
16
12
8
$E^*(^{24}Mg)$
$d^2\sigma/d\Omega\, dE^*$ (arb/sr.MeV)

Fig. 2

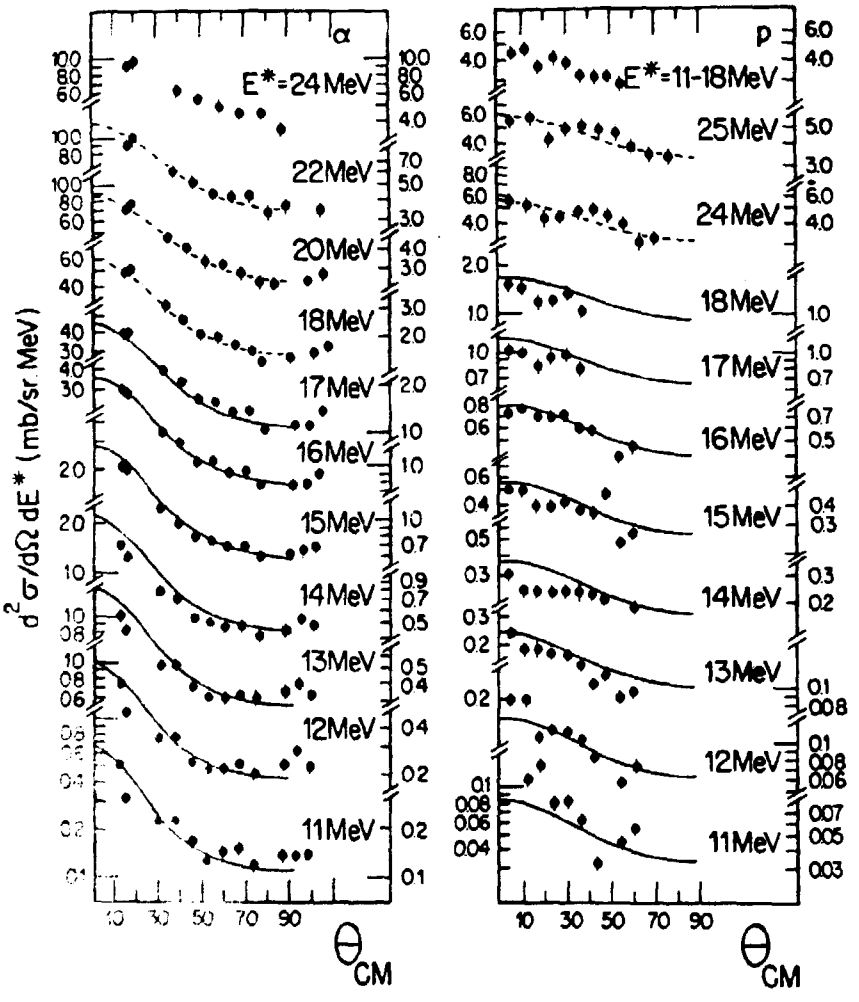
α
p
E*=24MeV
22MeV
20MeV
18MeV
17MeV
16MeV
15MeV
14MeV
13MeV
12MeV
11MeV
E*=11-18MeV
25MeV
24MeV
18MeV
17MeV
16MeV
15MeV
14MeV
13MeV
12MeV
11MeV
d²σ/dΩ dE* (mb/sr MeV)
θCM
θCM

Fig. 3

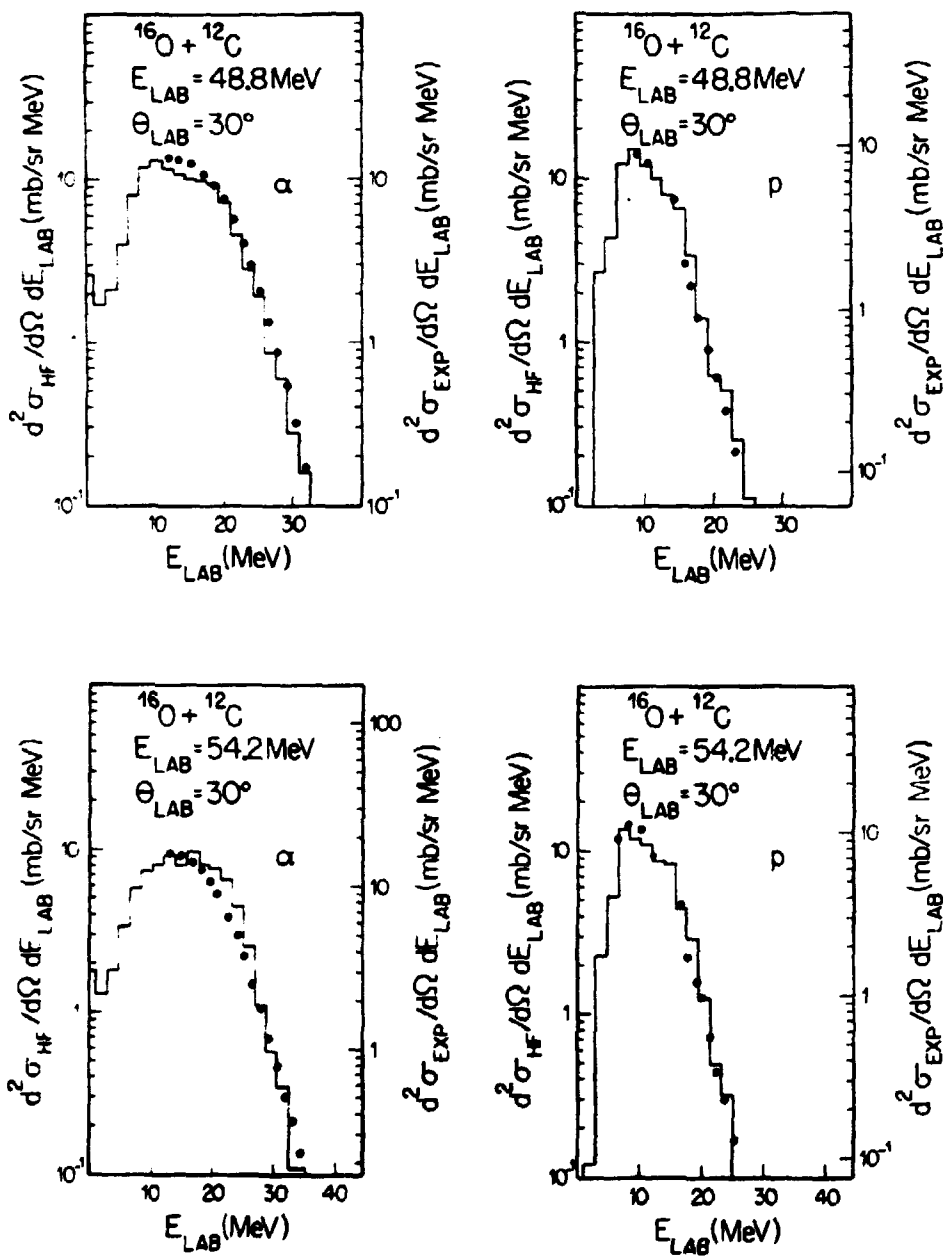
$^{16}O + ^{12}C$
$E_{LAB} = 48.8$MeV
$\theta_{LAB} = 30°$
α
p
$E_{LAB} = 54.2$MeV
$d^2\sigma_{HF}/d\Omega\, dE_{LAB}$ (mb/sr MeV)
$d^2\sigma_{EXP}/d\Omega\, dE_{LAB}$ (mb/sr MeV)
E_{LAB} (MeV)

Fig. 4

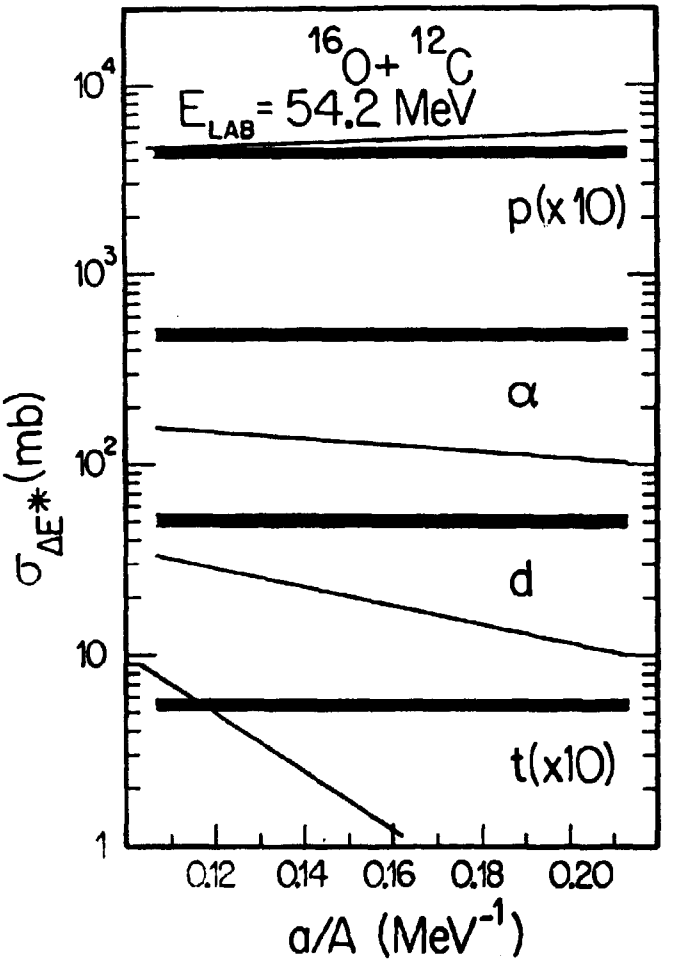
$^{16}O + ^{12}C$
E_{LAB} = 54.2 MeV
p(x10)
α
d
t(x10)
10^4
10^3
10^2
10
1
$\sigma_{\Delta E^*}$ (mb)
0.12
0.14
0.16
0.18
0.20
a/A (MeV^{-1})

Fig. 5

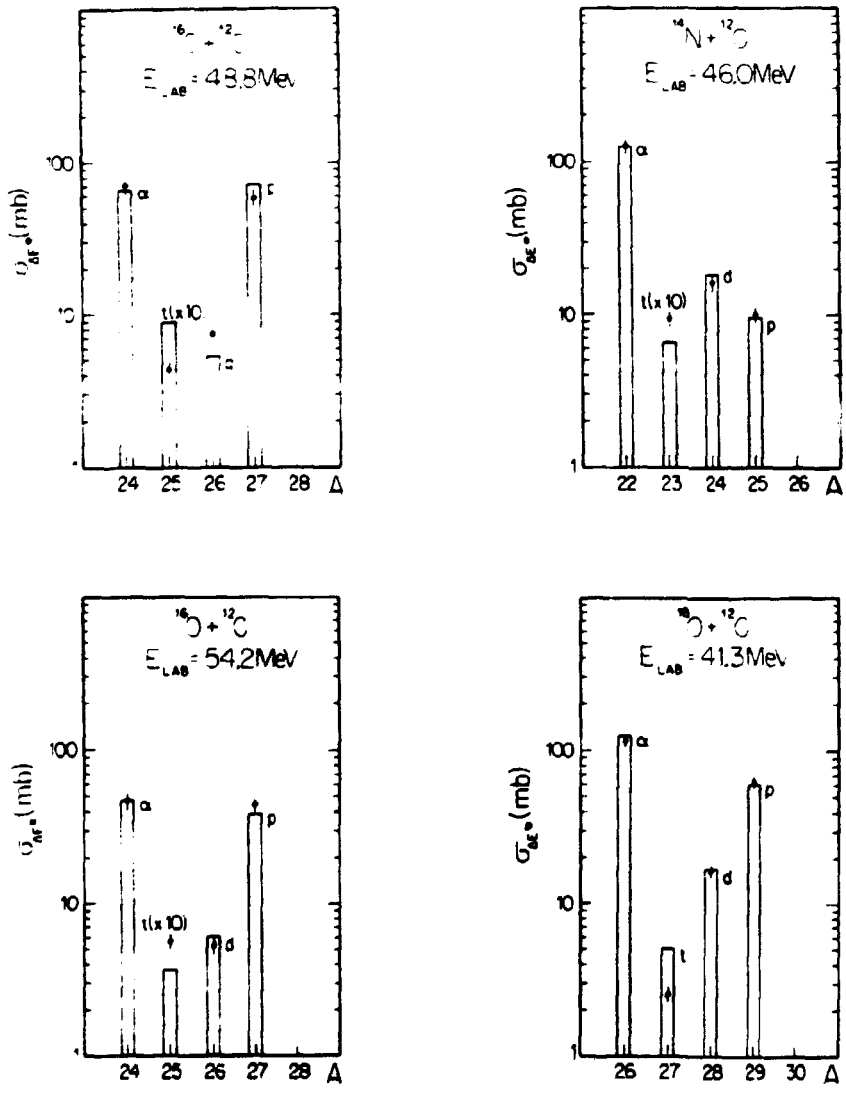
E_LAB = 43.8MeV
E_LAB = 46.0MeV
E_LAB = 54.2MeV
E_LAB = 41.3MeV
σ_ΔE•(mb)
100
10
1
t(x10)
a
d
p
24 25 26 27 28 A
22 23 24 25 26 A
26 27 28 29 30 A

Fig. 6

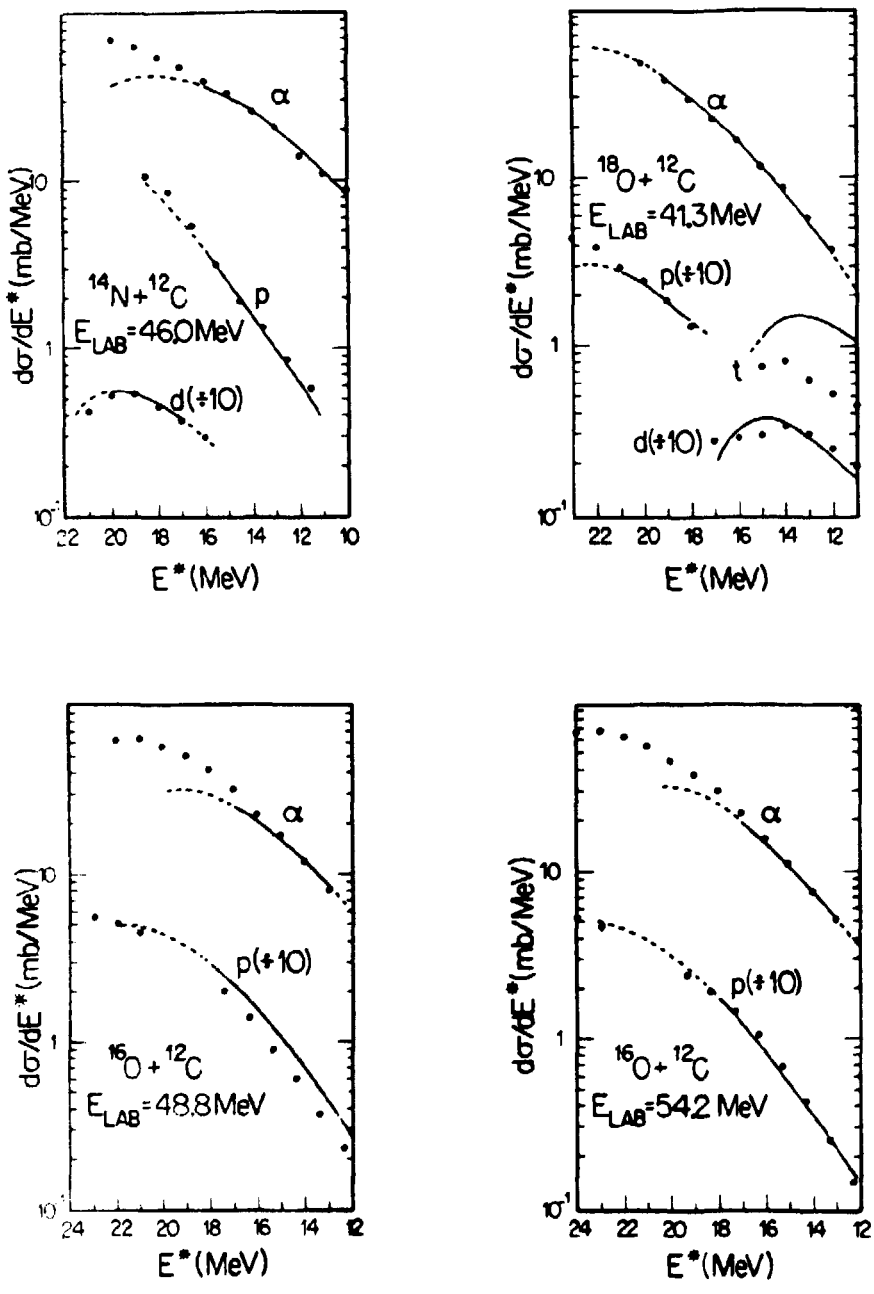
α
p
d(÷10)
$^{14}N+^{12}C$
E_{LAB}=46.0MeV
$d\sigma/dE^*$(mb/MeV)
E^*(MeV)
α
$^{18}O+^{12}C$
E_{LAB}=41.3MeV
p(÷10)
t
d(÷10)
$d\sigma/dE^*$(mb/MeV)
E^*(MeV)
α
p(÷10)
$^{16}O+^{12}C$
E_{LAB}=48.8MeV
$d\sigma/dE^*$(mb/MeV)
E^*(MeV)
α
p(÷10)
$^{16}O+^{12}C$
E_{LAB}=54.2 MeV
$d\sigma/dE^*$(mb/MeV)
E^*(MeV)

Fig. 7

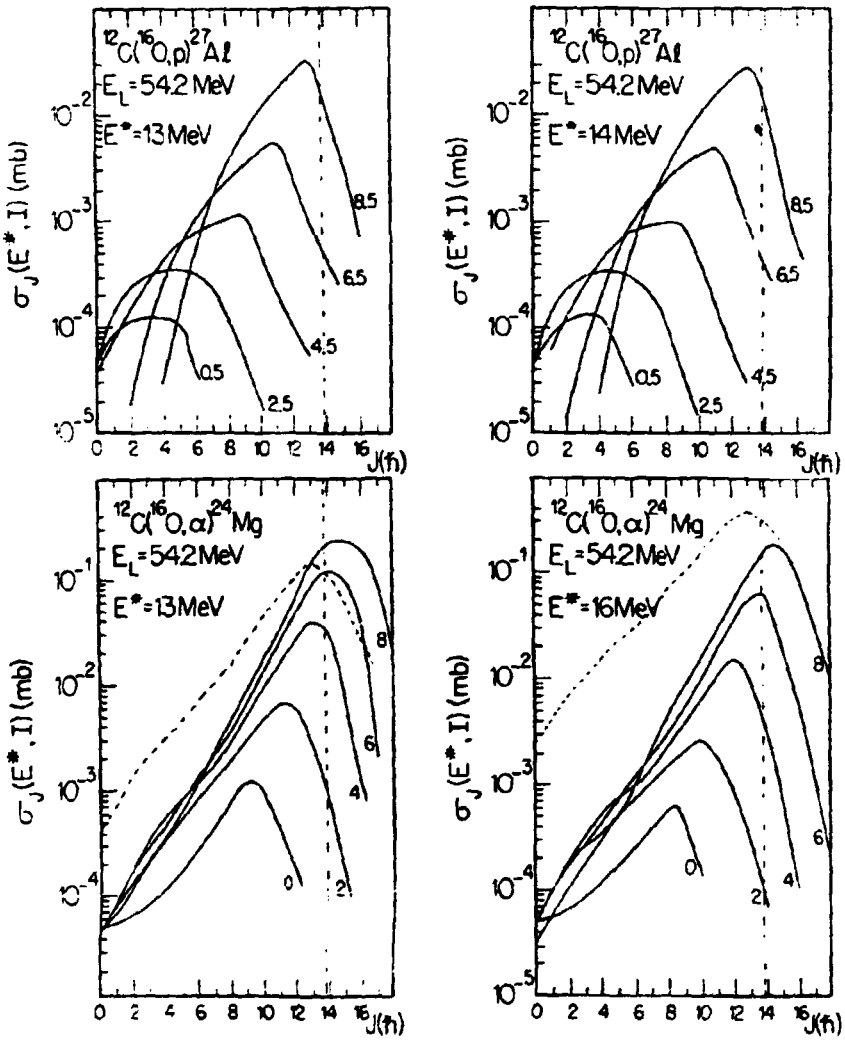
$^{12}C(^{16}O,p)^{27}Al$
E_L=54.2 MeV
E^*=13 MeV
E^*=14 MeV
$^{12}C(^{16}O,\alpha)^{24}Mg$
E^*=16 MeV
$\sigma_J(E^*,I)$ (mb)
J(ħ)
0.5
2.5
4.5
6.5
8.5
0
2
4
6
8

Fig. 8

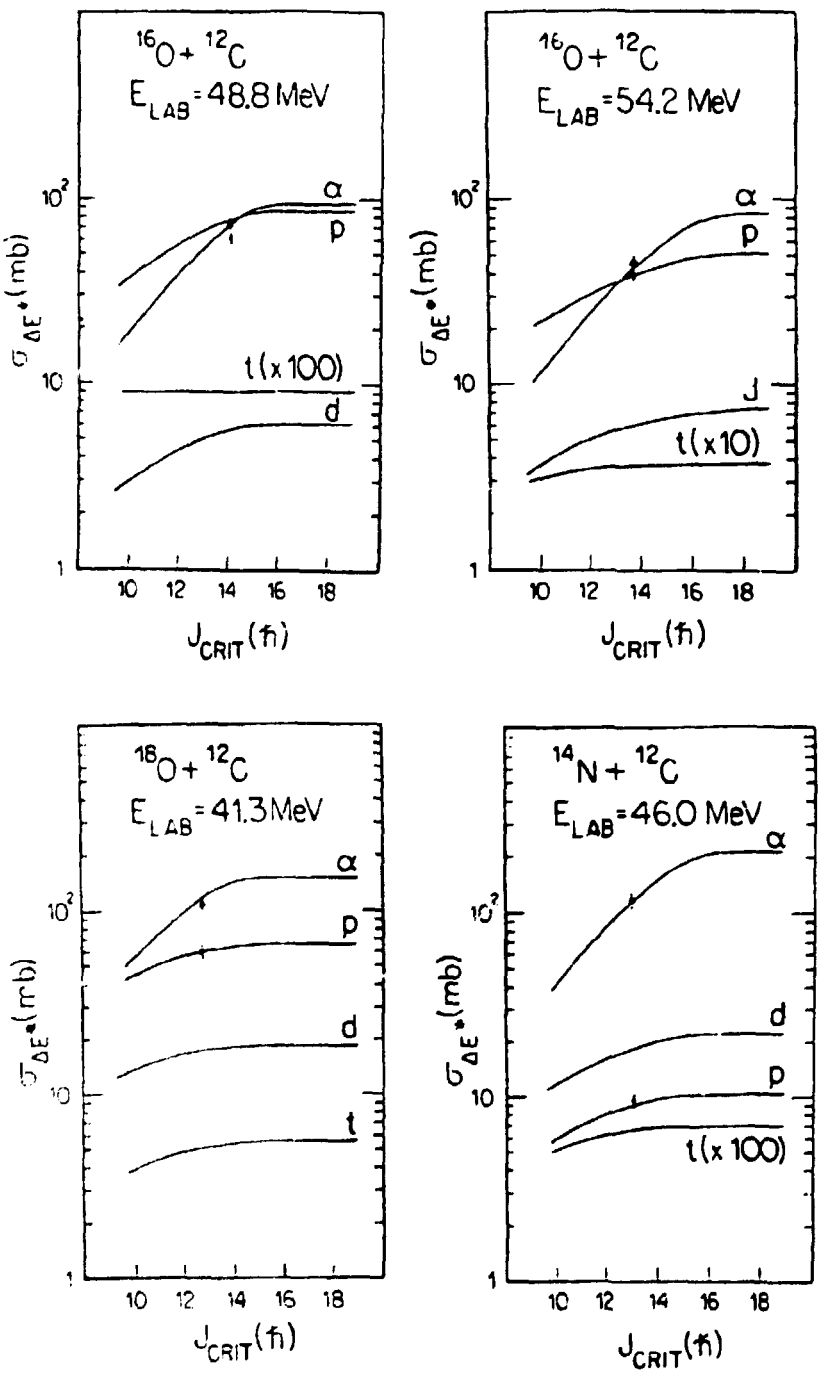
$^{16}O + ^{12}C$
$E_{LAB} = 48.8$ MeV
α
p
t(x100)
d
$\sigma_{\Delta E^*}$(mb)
$J_{CRIT}(\hbar)$
$^{16}O + ^{12}C$
$E_{LAB} = 54.2$ MeV
α
p
J
t(x10)
$\sigma_{\Delta E^*}$(mb)
$J_{CRIT}(\hbar)$
$^{18}O + ^{12}C$
$E_{LAB} = 41.3$ MeV
α
p
d
t
$\sigma_{\Delta E^*}$(mb)
$J_{CRIT}(\hbar)$
$^{14}N + ^{12}C$
$E_{LAB} = 46.0$ MeV
α
d
p
t(x100)
$\sigma_{\Delta E^*}$(mb)
$J_{CRIT}(\hbar)$

Fig. 9

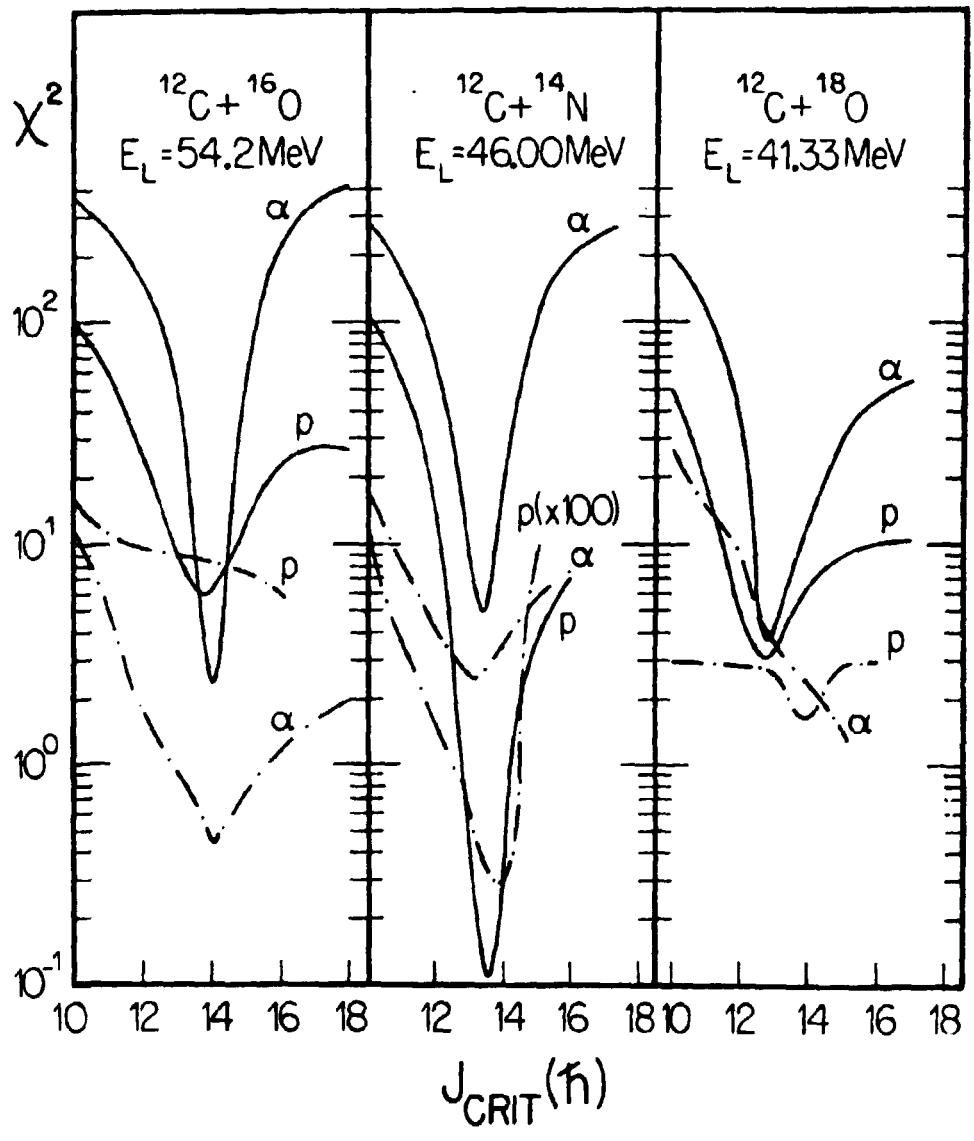
χ²
$^{12}C+^{16}O$
E_L=54.2MeV
$^{12}C+^{14}N$
E_L=46.00MeV
$^{12}C+^{18}O$
E_L=41.33MeV
α
p
p(x100)
10^2
10^1
10^0
10^{-1}
10 12 14 16 18
$J_{CRIT}(\hbar)$

Fig. 10

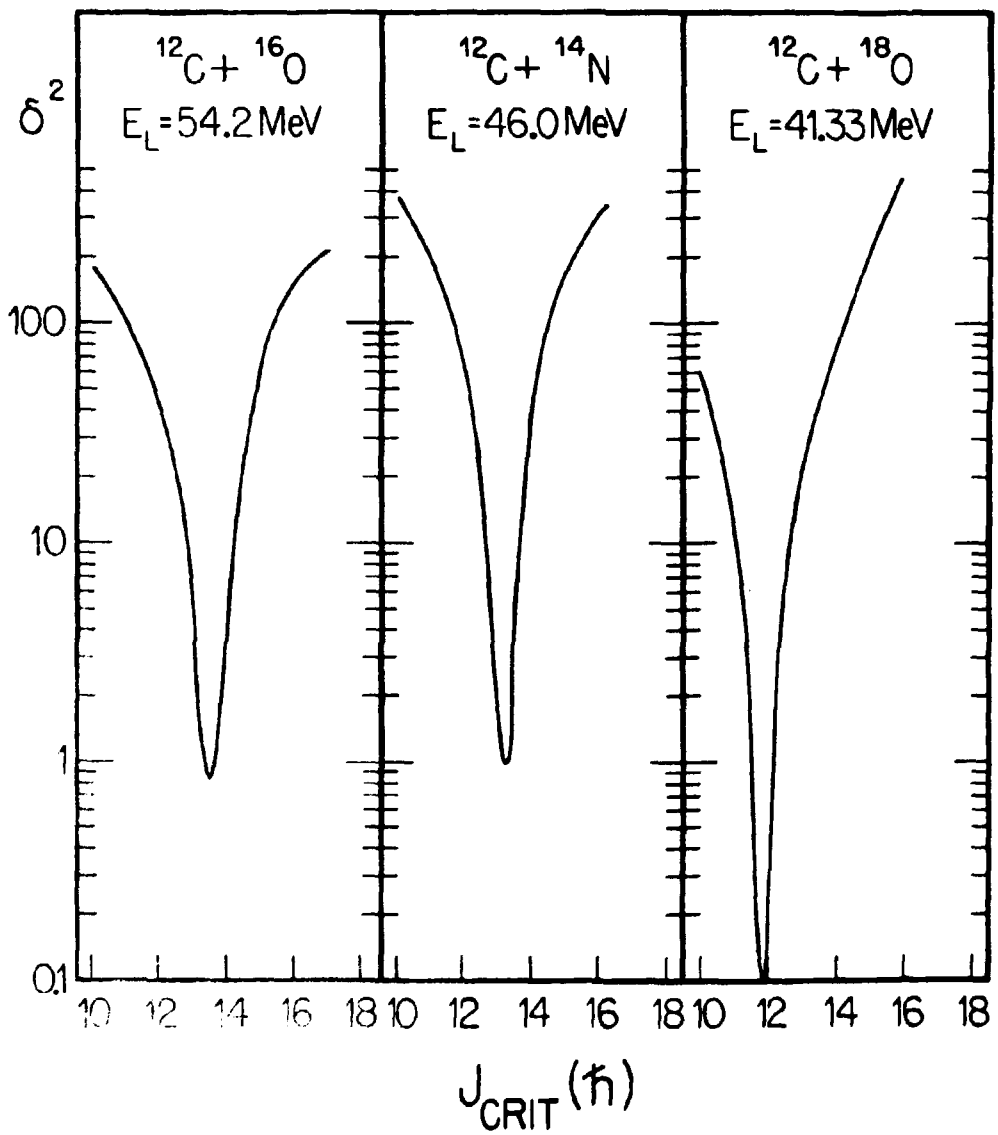
$^{12}C + ^{16}O$
$E_L = 54.2$ MeV
$^{12}C + ^{14}N$
$E_L = 46.0$ MeV
$^{12}C + ^{18}O$
$E_L = 41.33$ MeV
δ^2
100
10
1
0.1
10 12 14 16 18 10 12 14 16 18 10 12 14 16 18
$J_{CRIT}(\hbar)$

Fig. 11

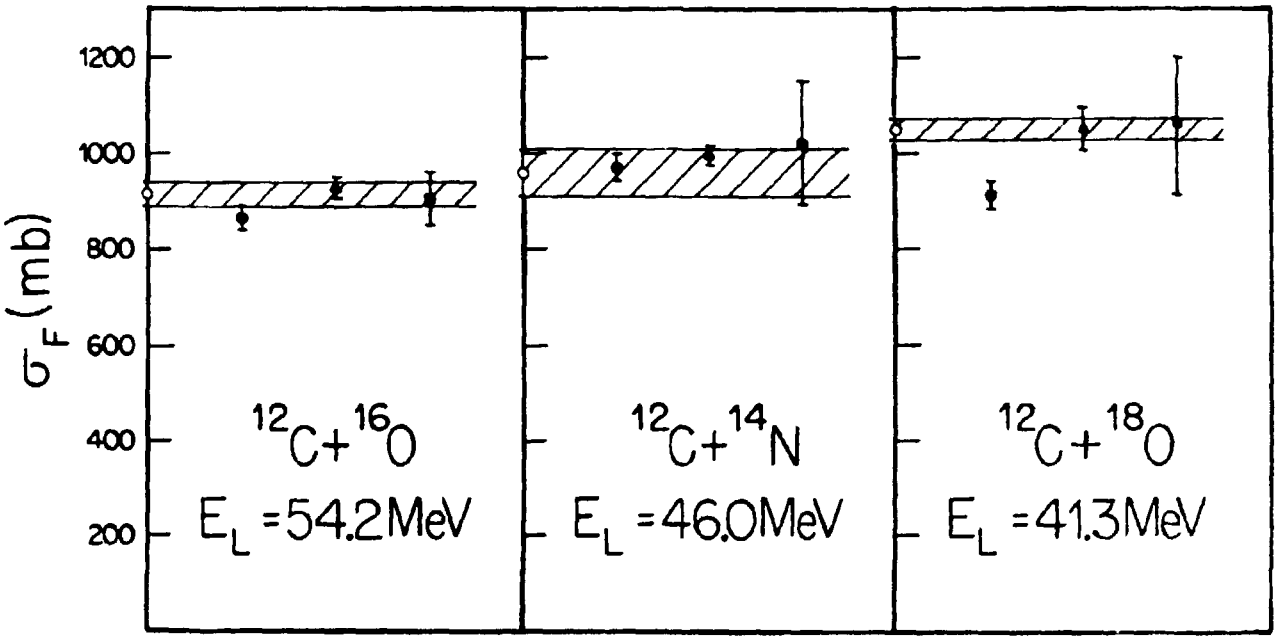
1200
1000
800
600
400
200
σ_F (mb)
$^{12}C+^{16}O$
E_L =54.2MeV
$^{12}C+^{14}N$
E_L =46.0MeV
$^{12}C+^{18}O$
E_L =41.3MeV

Fig. 12